

# Defining the $S_N1$ Side of Glycosylation Reactions: Stereoselectivity of Glycopyranosyl Cations

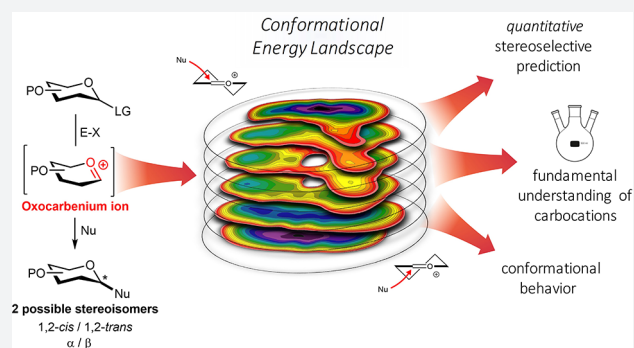
Thomas Hansen,<sup>†</sup> Ludivine Lebedel,<sup>‡</sup> Wouter A. Remmerswaal,<sup>†</sup> Stefan van der Vorm,<sup>†</sup> Dennis P. A. Wander,<sup>†</sup> Mark Somers,<sup>†</sup> Herman S. Overkleef,<sup>†</sup> Dmitri V. Filippov,<sup>†</sup> Jérôme Désiré,<sup>‡</sup> Agnès Mingot,<sup>‡</sup> Yves Bleriot,<sup>‡</sup> Gijsbert A. van der Marel,<sup>†</sup> Sebastien Thibaudeau,<sup>†</sup> and Jeroen D. C. Codée<sup>\*,†</sup>

<sup>†</sup>Leiden Institute of Chemistry, Leiden University, Einsteinweg 55, 2333 CC Leiden, The Netherlands

<sup>‡</sup>UMR-CNRS 7285, IC2MP, Equipe "Synthèse Organique", Université de Poitiers, 4 rue Michel Brunet, TSA 51106, Poitiers Cedex 9 86073, France

## Supporting Information

**ABSTRACT:** The broad application of well-defined synthetic oligosaccharides in glycobiology and glycobiochemistry is largely hampered by the lack of sufficient amounts of synthetic carbohydrate specimens. Insufficient knowledge of the glycosylation reaction mechanism thwarts the routine assembly of these materials. Glycosyl cations are key reactive intermediates in the glycosylation reaction, but their high reactivity and fleeting nature have precluded the determination of clear structure–reactivity–stereoselectivity principles for these species. We report a combined experimental and computational method that connects the stereoselectivity of oxocarbenium ions to the full ensemble of conformations these species can adopt, mapped in conformational energy landscapes (CEL), in a quantitative manner. The detailed description of stereoselective  $S_N1$ -type glycosylation reactions firmly establishes glycosyl cations as true reaction intermediates and will enable the generation of new stereoselective glycosylation methodology.



Carbohydrates play numerous roles in living organisms, as key players in energy housekeeping, as structural components, and as signaling molecules. To unravel the roles carbohydrates play in biological processes, well-defined, single molecules are indispensable, and organic synthesis has been one of the major suppliers for pure oligosaccharide specimens to fuel glycobiological and glycomedical research. Although significant progress has been made in the field, the generation of sufficient amounts of synthetic (complex) oligosaccharides remains a difficult and time-consuming undertaking.<sup>1–5</sup> The main obstacle in the construction of oligosaccharides is the stereoselective construction of 1,2-*cis*-glycosidic linkages.<sup>6,7</sup> While 1,2-*trans* linkages can be reliably installed using a neighboring group participation approach, there is no general solution for the construction of 1,2-*cis* linkages. Different reaction pathways can be followed during a glycosylation reaction, and these can lead to different diastereomeric products. Figure 1 depicts the current understanding of the continuum of mechanisms that is operational during a glycosylation reaction.<sup>8–10</sup> The activation of a donor glycoside (I) leads to an array of reactive (electrophilic) intermediates (II–VIII), formed from the donor glycoside and the activator-derived counterion. In case a participating group is present at the C2 (such as an *O*-acyl function), these reactive

intermediates are intramolecularly trapped to provide a relatively stable dioxolenium ion, that is stereoselectively substituted from the opposite side of the ring to deliver the 1,2-*trans* glycoside product. In the absence of a C2-participation functionality, the situation is more complex, and it has been proposed that both covalent reactive intermediates (II and VIII) and the reactive oxocarbenium ion (like) species (III–VII) can be the product-forming intermediates. The covalent intermediates on the  $S_N2$  side of the reaction mechanism continuum can be studied using low-temperature NMR techniques, and over the years, hundreds of reactive intermediates (triflates, oxosulfonium ions, among others) have been characterized.<sup>11–18</sup> Substitution of these species with reactive nucleophiles (such as primary carbohydrate alcohols) defines the  $S_N2$  side of the reaction mechanism continuum. In contrast, the oxocarbenium ions on the  $S_N1$  side of the continuum remain ill understood, and the intermediacy of these species in glycosylation reactions is heavily debated.<sup>19–36</sup> Because the lifetime of these intermediates in conventional reaction media is extremely short, there is currently no (spectroscopic) technique available to study

Received: January 15, 2019

Published: April 18, 2019

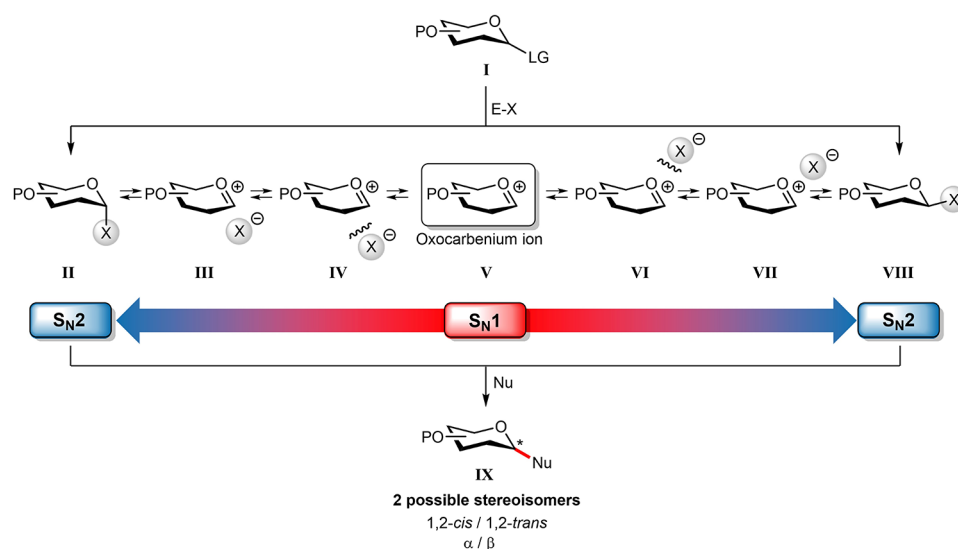


**Figure 1.** The reaction mechanism manifold operational during glycosylation reactions. Glycosylation reactions are best considered as taking place at a continuum between two formal extremes of the mechanisms, including the  $S_N1$  and  $S_N2$  mechanism. (I) Donor substrate; (II) reactive covalent  $\alpha$ -intermediate; (III) contact ion pair, with the leaving group associated at the  $\alpha$ -face; (IV) solvent-separated ion pair, with the leaving group that has departed from the  $\alpha$ -face; (V) solvent-separated oxocarbenium ion; (VI) solvent-separated ion pair, with the leaving group that has departed from the  $\beta$ -face; (VII) contact ion pair, with the leaving group associated at the  $\beta$ -face; (VIII) reactive covalent  $\beta$ -intermediate; and (IX) addition product. P, protection group; E-X, promoter system; and Nu, nucleophile.

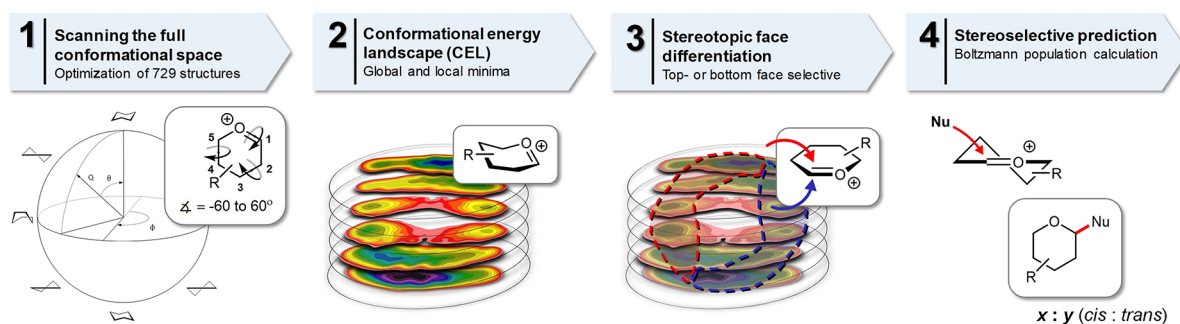


**Figure 2.** Overview of the workflow to map the conformational and stereoselective preference of pyranosyl oxocarbenium ions. (1) The complete conformational space of a six-membered ring was scanned by computing 729 prefixed structures. A few canonical conformations (chair, half-chair, envelope, and boat) are depicted. (2) The associated energies were graphed on slices dividing the Cremer–Pople sphere. (3) Top- and bottom-face selective conformers lie in separate areas of the sphere. The family of the top face-selective ( ${}^3E$ ,  ${}^3H_4$ ,  $E_4$ , and  $B_{2,5}$ )-like structures is found in the area contoured with the red-dashed line, while the bottom face-selective family of ( ${}^4E$ ,  ${}^4H_3$ ,  $E_3$ , and  ${}^{2,5}B$ )-like conformers is found on the opposite side of the sphere, grouped within the blue-dashed line. (4) On the basis of the Boltzmann distribution of the top- and bottom-face selective structures, the stereochemical outcome of nucleophilic addition reactions to pyranosyl oxocarbenium ions can be computed.

these species in a direct manner and assess their behavior.<sup>37–39</sup> It is clear that the substitution pattern on the carbohydrate ring plays an all-important role in determining the stability and reactivity of these species, but it has been impossible to establish clear structure–reactivity–stereoselectivity relationships because of the conformational freedom and short lifetime of these reactive intermediates in classical solutions. Thus, the course of  $S_N1$ -type glycosylation can, at present, not be properly understood (let alone predicted), leaving a major gap in the mechanistic conception of glycosylation reactions.

To investigate the stability and reactivity of glycosyl oxocarbenium ions as product forming intermediates in glycosylation reactions, we here report the development of a computational method that maps the stability of these species as a function of their overall shape. We show that the stereoselectivity of glycosylation reactions employing weak nucleophiles can be directly related to the conformational

energy landscape (CEL) of the glycosyl oxocarbenium ions, as mapped *in silico*, and in doing so, define the  $S_N1$  side of the glycosylation reaction mechanism manifold. Direct spectroscopic evidence for the computed conformers is obtained by the generation of the oxocarbenium ions under superacid conditions, and it is here revealed that fully substituted glycopyranosyl oxocarbenium ions react in a highly stereoselective 1,2-*cis* manner.

We have mapped the energy of glycopyranosyl oxocarbenium ions as a function of their shape to understand the reactivity of these species following the strategy outlined in Figure 2. To generate the CEL maps, plotted on the Cremer–Pople sphere (a spherical representation describing all possible conformations a six-membered ring can adopt), we have generated a suite of conformations by scanning the three dihedral angles (C1–C2–C3–C4, C3–C4–C5–O5, and C5–O5–C1–C2) from  $-60^\circ$  to  $60^\circ$  in  $15^\circ$  increments, to

**Table 1. Computed and Experimentally Found Stereoselectivity for Glycosylation Reactions on Mono- and Multi-Substituted Pyranosyl Oxocarbenium Ions<sup>56</sup>**

Entry	oxocarbenium ion	computed stereoselectivity ( <i>cis:trans</i> ) <sup>a</sup>	experimental stereoselectivity ( <i>cis:trans</i> ) <sup>a</sup>	yield (%)
1	1 (4-OBn)	<2:98	<2:98	75
2	2 (4-F)	<2:98	4:96	45
3	3 (4-OTBDPS)	8:92	6:94	99
4	4 (4-N <sub>3</sub> )	12:88	12:88	95
5	5 (4-Cl)	10:90	14:86	90
6	6 (4-Br)	32:68	29:71	87
7	7 (4-I)	73:27	72:28	90
8	8 (4-SPh)	81:19	78:22	87
9	9 (4-SMe)	88:12	84:16	75
10	10 (4-Me)	95:5	94:6	74
11	11 (3-OBn)	90:10	92:8	95
12	12 (3-Me)	4:96	3:97	41
13	13 (2-OBn)	66:34	66:34	85
14	14 (D-lyxose)	>98:2	>98:2	81
15	15 (D-arabinose)	>98:2	>98:2	79
16	16 (D-xylose)	>98:2	>98:2	86
17	17 (2-deoxy-D-xylose)	>98:2	>98:2	74
18	18 (D-ribose)	>98:2	>98:2	69
19	19 (L-fucose)	>98:2	>98:2	74
20	20 (2-deoxy-L-fucose)	<2:98	<2:98	89
21	21 (2-azido-L-fucose)	>98:2	>98:2	65
22	22 (L-rhamnose)	>98:2	>98:2	79
23	23 (2-deoxy-L-rhamnose)	71:29	66:34	96
24	24 (D-glucose)	>98:2	>98:2	70
25	25 (D-glucuronic acid)	>98:2	>98:2	43
26	26 (2-deoxy-D-glucose)	52:48	52:48	76
27	27 (2-azido-D-glucose)	>98:2	>98:2	52
28	28 (D-mannose)	97:3	97:3	93
29	29 (D-mannuronic-acid)	>98:2	>98:2	76
30	30 (2-azido-D-mannuronic-acid)	>98:2	>98:2	53
31	31 (D-galactose)	>98:2	>98:2	86
32	32 (2-deoxy-D-galactose)	<2:98	<2:98	91

<sup>a</sup>For the monosubstituted pyranosides (entries 1–13), the *cis:trans* ratio is expressed as the relationship between the substituent and the coupled nucleophile. For the 2-deoxy-glycosides (entries 17, 20, 23, and 32), the *cis:trans* ratio is expressed as the relationship between the substituent on C-3 and the coupled nucleophile. For the other glycopyranosides (entries 14–16, 18–19, 21–22, and 27–31), the *cis:trans* ratio is expressed as the relationship between the substituent on C-2 and the coupled nucleophile. The names in the table relate to the carbohydrate studied. For the computational studies, per-*O*-methylated oxocarbenium ions are used, where the experimental glycosylation used per-*O*-benzylated substrates.<sup>57</sup>

fill the complete conformation space (Figure 2,1). The geometry of all these conformers was optimized, and the associated energies were computed by utilizing DFT as the level of theory, B3LYP as hybrid functional,<sup>40</sup> and 6-311G(d,p) as the basis set. Solvation of CH<sub>2</sub>Cl<sub>2</sub> was taken into account using a polarizable continuum model, and energies are expressed in Gibbs free energy (for more information, see the Supporting Information).<sup>41</sup> The energy landscapes were then generated by visualizing the relative energy in contour plots on “slices” of the pseudo rotational sphere.<sup>42</sup>

Inspection of the generated energy maps revealed that two families of structures are most relevant, the continuum of (<sup>3</sup>E, <sup>3</sup>H<sub>4</sub>, E<sub>4</sub>, and B<sub>2,5</sub>)-like structures is grouped on the northwest side of the spheres, and these form an ensemble of structures that are preferentially attacked from the top-face. The “opposite” family of structures, located on the southeast side of the sphere, is composed of the range of (<sup>4</sup>E, <sup>4</sup>H<sub>3</sub>, E<sub>3</sub>, and <sup>2,5</sup>B)-like conformers, which will likely be approached by an incoming nucleophile from the bottom-face (see Figure 2,3 and the Supporting Information).<sup>20,43</sup> The relative population of all conformational states can be calculated, on the basis of

their relative energies as computed above, utilizing the Boltzmann equation (see the Supporting Information for more information). Accordingly, we determined the population of the top- and bottom-face selective families, which should be a measure for the relative stereoselectivity of addition reactions with weak nucleophiles to the glycosyl oxocarbenium ions.

To put this workflow to practice, we first investigated a set of 13 monosubstituted pyranosyl oxocarbenium ions differing by the nature of the substituent (BnO–, TBDPSO–, N<sub>3</sub>–, F–, Cl–, Br–, I–, PhS–, MeS–, and Me–) as well as the position on the ring. Their structures, the computed theoretical reaction stereoselectivity, and the experimentally determined stereoselectivity obtained in reactions with triethylsilane-*d* (TES-D)<sup>19,44–46</sup> or allyl-trimethyl silane (AllylTMS) are summarized in Table 1 (entries 1–13). The CEL maps (see Figure 3a for three representative examples, all other CEL maps are provided in Figures S3–18) revealed that only a limited region of the full conformational space is accessible for the monosubstituted ions, in which local minima are found at both “poles”, centered around the <sup>3</sup>H<sub>4</sub>- and the <sup>4</sup>H<sub>3</sub>-like con-

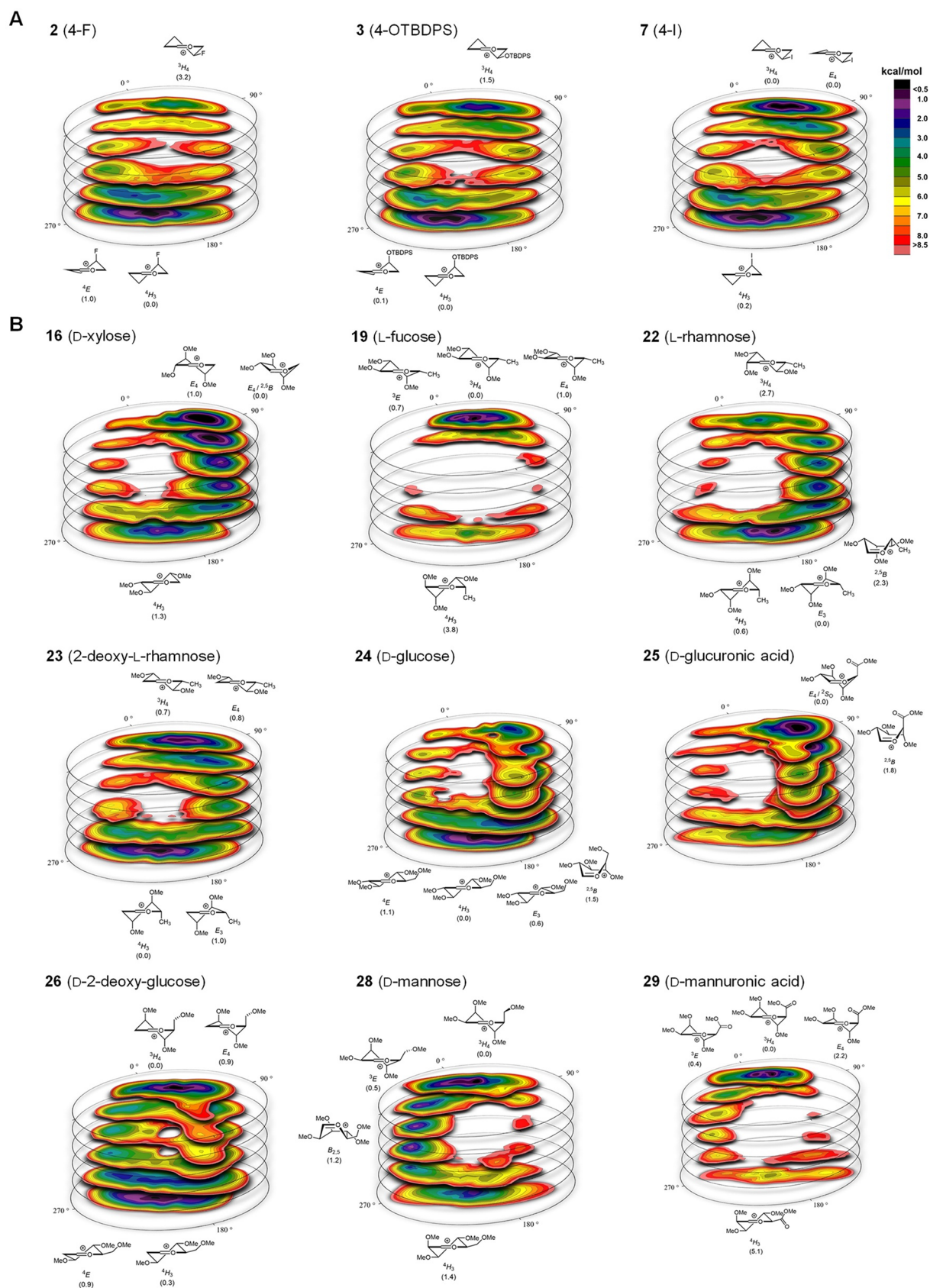


**Figure 3.** CEL maps of selected pyranosyl oxocarbenium ions in which the found local minima are indicated with their respective energy. (A) CEL map of monosubstituted-pyranosyl oxocarbenium ions 2, 3, and 7. (B) CEL map of multi-substituted-pyranosyl oxocarbenium ions 16, 19, 22–26, and 28–29.

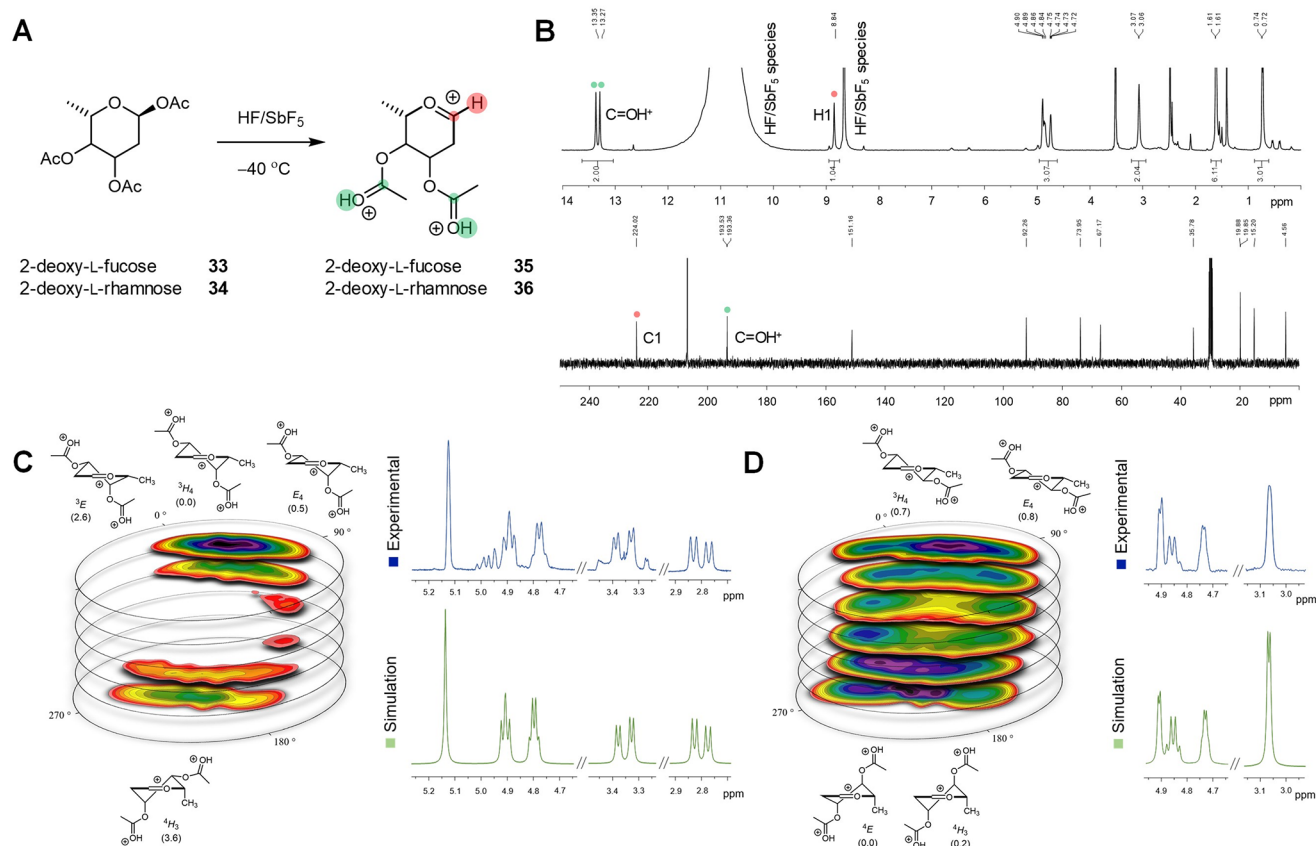


**Figure 4.** Generation and NMR spectra of 2-deoxy-pyranosyl oxocarbenium ions in HF/SbF<sub>5</sub> at -40 °C. (A) Generation of ion **35** and **36** in HF/SbF<sub>5</sub>. (B) Experimental <sup>1</sup>H- and <sup>13</sup>C DEPT NMR of 2-deoxy-L-rhamnose oxocarbenium **34**. (C) The generated <sup>1</sup>H NMR spectrum of the oxocarbenium **35** compared to the simulated spectrum based on the computed CEL. (D) The generated <sup>1</sup>H NMR spectrum of the oxocarbenium **36** compared to the simulated spectrum based on the computed CEL.

formations. Depending on the nature of the substituents, one of these families is favored, placing the substituent either axially or equatorially. At the C4-position, electronegative substituents (BnO-, F-, TBDPSO-, N<sub>3</sub>-, Cl-, and Br-) favor an axial position to stabilize the oxocarbenium ion by through space electrostatic interactions, preferentially adopting the <sup>4</sup>H<sub>3</sub>-like conformation.<sup>31,32,47–49</sup> Decreasing electronegativity and increasing size of the substituent (I-, PhS-, MeS-, and Me-) translates to a preference to adopt an equatorial position (<sup>3</sup>H<sub>4</sub>-like conformations) to minimize steric interactions (Figure 3a). This trend is similar for substituents at the C3-position. An electronegative BnO-substituent at C-2 is preferentially placed in a *pseudo*-equatorial position, as this enables the hyperconjugative stabilization of the oxocarbenium ion by the *pseudo*-axial C2–H2 bond. When the population of the conformational families, as revealed in the CEL maps, are translated to a calculated stereoselectivity and compared to the stereoselectivity obtained in the experiments,<sup>31,32,50</sup> it becomes apparent that there is an excellent agreement between theory and practice. Importantly, not only can highly stereoselective glycosylations be reliably predicted from the CEL maps, but also the condensation reactions that proceed with moderate selectivity (Table 1, entries 6, 7, and 13 for example) are accurately matched by the computed data.

Next, CEL maps of multisubstituted pyranosyl oxocarbenium ions were generated, and the theoretical stereoselectivity of these species were computed. The results of these studies are summarized in the second half of Table 1 (entries 14–32).

A selection of CEL maps is depicted in Figure 3b (all CEL maps are provided in Figures S22–40). Table 1 also reports the experimental stereoselectivity and yield of the reactions of the thioglycoside donors, obtained by preactivation of the donors using the diphenyl sulfide (Ph<sub>2</sub>SO)/triflic anhydride (Tf<sub>2</sub>O) activator<sup>51</sup> and TES-D as the nucleophile.<sup>52</sup> Again, an excellent agreement is found for the calculated and experimentally obtained stereoselectivity. The stereoselectivity of all these condensation reactions can now be traced back to the families of low-energy conformers of the oxocarbenium ions, as revealed by the CEL maps. Some maps show a very localized energy minimum for a particular conformational family, such as the CEL map for the L-fucosyl oxocarbenium ion **19** (Figure 3b). In the most favorable <sup>3</sup>H<sub>4</sub>-, <sup>3</sup>E-, and E<sub>4</sub>-like conformations of this ion, the ring substituents at C2 and C4 take up an electronically favorable orientation, leading to the localized energy minimum around the <sup>3</sup>H<sub>4</sub>-pole. Nucleophilic addition to these conformers stereoselectivity provides the 1,2-*cis*-linked products, and the generated CEL map thus provides an explanation for the high 1,2-*cis*-selectivity generally observed with fucosyl donors.<sup>53–55</sup>

Similarly, the mannosyl oxocarbenium ion **28** can place its C2, C3, and C4 substituents in stabilizing positions when adopting a <sup>3</sup>H<sub>4</sub>/<sup>3</sup>E-like structure (Figure 3b), as alluded to by Woerpel and co-workers.<sup>24</sup> These structures are selectively substituted from the top face to provide the mannosyl product, a result that is indeed born out in the glycosylation experiment (Table 1, entry 28). Glycosylations of mannanuronic acid ester

**29** proceed with exceptional 1,2-*cis* stereoselectivity, and the generated CEL map (Figure 3b) provides an adequate explanation for this reaction outcome, as a very localized energy minimum is determined for the  $^3H_4$ -like conformational family. The additional stabilization from the axial C5-CO<sub>2</sub>Me in **29** with respect to the axial C5-CH<sub>2</sub>OMe group in the mannosyl oxocarbenium ion (**28**) becomes very clear from the comparison of the CEL maps of **28** and **29**.

The CEL maps of pyranosyl oxocarbenium ions bearing substituents that have “conflicting positional interests” reveal that noncanonical conformations can become important, and that broader conformational families or families around the different poles can become equally relevant. For example, the D-xylosyl oxocarbenium ion **16** preferentially adopts a noncanonical flattened (skew)-boat-like structure (see Figure 3b). The CEL map for the 2-deoxy-L-rhamnose ion **23** reveals two conformational families of similar energy, leading to a mixture of  $\alpha$ - and  $\beta$ -products in the condensation reaction (Table 1, entry 23). The CEL maps in the *gluco*-series illustrate how point mutations in the structure of the parent donor translate to differently shaped oxocarbenium ions and a different stereochemical outcome in the glycosylation reactions. The glucopyranosyl cation **24** is most stable when adopting a  $^4H_3/E_4$ -like shape, while its glucuronic acid counterpart (**25**), bearing a C5-carboxylic acid ester, prefers to adopt a structure in between the  $E_4$  and  $^2S_0$ -conformations. Both ions are preferentially attacked from the bottom-face to selectively provide the  $\alpha$ -product (Table 1, entries 24 and 25). For 2-deoxyglucose **26**, two families of oxocarbenium ion conformers are equally stable, and the population of  $^4H_3/E_4$ -like and  $^3H_4/E_4$ -like states leads to an unselective addition reaction, leading to the formation of  $\alpha$ - and  $\beta$ -products in almost equal amounts.

Overall, there is an excellent agreement between the calculated and experimentally established  $\alpha/\beta$ -selectivity of the multi-substituted glycosides, providing very compelling evidence for (families of) glucopyranosyl oxocarbenium ion conformers as product-forming intermediates in the substitution reactions; thereby defining the S<sub>N</sub>1 side of the glycosylation reaction mechanism manifold.

To obtain direct experimental evidence for the conformations computed using our CEL mapping method, we studied two 2-deoxy diacetylated oxocarbenium ions derived from L-fucose **33** and L-rhamnose **34** in “non-nucleophilic” superacidic media (Figure 4a).<sup>37</sup> The choice of the acetyl group and 2-deoxy position is guided by the fact that methoxy groups are prone to elimination, and so far, C-2 substituents able to provide the corresponding glycosyl cation are limited. As the acetyl groups at C-3 and C-4 of the oxocarbenium ions generated from donors **33** and **34** will be protonated under the superacidic conditions used, polycationic oxocarbenium ions **35** and **36** were subjected to the CEL mapping method. The CEL map for 2-deoxy-fucosyl oxocarbenium ion **35** (Figure 4c) shows a strong preference for the  $^3H_4$  and closely related  $E_4$  conformations. The CEL map for the 2-deoxy-rhamnosyl oxocarbenium ion **36**, on the other hand, features multiple local minima, and both the  $^3H_4$  and the  $^4H_3$  family are relatively low in energy, resulting in a conformational mixture in solution. In parallel, 2-deoxy-L-fucose and 2-deoxy-L-rhamnose acetates **33** and **34** were dissolved in HF/SbF<sub>5</sub> to generate the polycationic structures **35** and **36**, of which the NMR spectra (Figure 4b) clearly indicated the presence of an oxocarbenium ion as the main species (carboxonium signal 35:

$\delta_{C1} = 223.4$  ppm and  $\delta_{H1} = 8.76$  ppm; **36**:  $\delta_{C1} = 224.2$  ppm and  $\delta_{H1} = 8.84$  ppm).<sup>37,58</sup> Both ester groups were indeed protonated, as revealed by the presence of two proton singlets at  $\delta_H = 13.27$  and 13.35 ppm. Because of the sufficient lifespan of **35** and **36** in the superacid media, full conformational characterization of these species could be performed (see the SI for more information). The coupling constants of the ring protons of **35** indicate that it adopts a stable  $^3H_4$ -like conformation. The NMR spectrum of 2-deoxy-L-rhamnosyl oxocarbenium **36** (Figure 4d), on the other hand, showed significant line broadening as a result of conformational flexibility of this species. Using the relevant conformations, obtained from the CEL maps for these ions, we reconstituted the NMR spectrum using the Boltzmann weighted averaged coupling constants of ions **35** and **36**. Perfect agreement between the experimental NMR spectra for these peracetylated polyprotonated glycosyl cations and their simulated spectra show that conformational dynamics of these ions are well captured by the CEL mapping method.

In conclusion, we have benchmarked the S<sub>N</sub>1 side of the glycosylation reaction mechanism. The stability, reactivity, and conformational mobility of glycosyl oxocarbenium ions can be fully understood by mapping the complete conformational energy landscape of these ions, and the preference of the cations can be directly related to the experimental stereochemical outcome of addition reactions to these. The maps show, in detail, how the stereoelectronic effects of various ring substituents (halogens, chalcogens, azides, and carbon-based substituents) determine the overall shape of the cations and thereby the stereochemical course of the reactions. In addition, the simulated NMR spectra of selected ions, reconstituted by using the Boltzmann weighted averaged coupling constants determined by the CEL mapping method, perfectly fit with the experimental ones observed by low-temperature NMR in superacid. Where glycosyl oxocarbenium ions were previously thought to be at the basis of nonselective coupling reactions because of their high reactivity, we here show that these species, including the ions derived from L-fucose, L-rhamnose, D-glucose, D-mannose, and D-galactose, have an intrinsic preference to generate the challenging 1,2-*cis*-linkages. This will enable the stereoselective synthesis of C-glycosides and open up new avenues to develop stereoselective O-glycosylation reactions.<sup>59</sup> The mechanistic insight offered here will be instrumental in the interpretation of future glycosylation results and serve as the basis to further explore the glycosylation reaction mechanism. The uncovered stereoelectronic substituent effects will be relevant in many other transformations, involving carbocationic intermediates, and the strategy that we developed to grasp the full conformational space of these flexible intermediates can be a blueprint for the study of other flexible reactive intermediates.

## ■ ASSOCIATED CONTENT

### Supporting Information

The Supporting Information is available free of charge on the ACS Publications website at DOI: 10.1021/acscentsci.9b00042.

Experimental and computational procedures, CEL maps of all studied ions, construction of CEL maps, additional experiments with methyl ether-protected substrates, different solvent systems and donor types, coordinates of all most relevant low energy oxocarbenium ion

conformers, and NMR spectra of all new and selected compounds (PDF)

## AUTHOR INFORMATION

### Corresponding Author

\*E-mail: [jcodee@chem.leidenuniv.nl](mailto:jcodee@chem.leidenuniv.nl)

### ORCID

Thomas Hansen: 0000-0002-6291-1569

Wouter A. Remmerswaal: 0000-0002-1040-4311

Stefan van der Vorm: 0000-0002-4047-9373

Dennis P. A. Wander: 0000-0003-3881-5240

Herman S. Overkleeft: 0000-0001-6976-7005

Dmitri V. Filippov: 0000-0002-6978-7425

Yves Bleriot: 0000-0002-3209-9282

Sebastien Thibaudeau: 0000-0002-6246-5829

Jeroen D. C. Codée: 0000-0003-3531-2138

### Author Contributions

T.H. and J.D.C.C. conceived the project, designed the experiments, and composed the manuscript. T.H. generated the CEL maps and analyzed the data. T.H. carried out the donor synthesis and the coupling experiments. W.A.R., S.V., and D.P.A.W. contributed to the donor synthesis. Y.B. and S.T. designed the superacid experiments. L.L. and A.M. performed all superacid experiments. All authors commented on the manuscript.

### Funding

Computing resources have been provided by BigGrid.nl and SURFsara. We thank the European Research Council (ERC-CoG-726072-“GLYCONTROL”, to J.D.C.C.) and EP Nuffic (Van Gogh grant to T.H.) for financial support. We also thank the CNRS, the University of Poitiers, the National Research Agency (ANR project SWEETCAT), and Campus France (PHC Van Gogh 2017) for financial support to L.L., A.M., J.D., Y.B., and S.T.

### Notes

The authors declare no competing financial interest.

## REFERENCES

- (1) Zhu, X.; Schmidt, R. R. New Principles for Glycoside-Bond Formation. *Angew. Chem., Int. Ed.* **2009**, *48* (11), 1900–1934.
- (2) Seeberger, P. H. The Logic of Automated Glycan Assembly. *Acc. Chem. Res.* **2015**, *48* (5), 1450–1463.
- (3) Wang, C. C.; Lee, J. C.; Luo, S. Y.; Kulkarni, S. S.; Huang, Y. W.; Lee, C. C.; Chang, K. L.; Hung, S. C. Regioselective One-Pot Protection of Carbohydrates. *Nature* **2007**, *446* (7138), 896–899.
- (4) Leng, W.; Yao, H.; He, J.; Liu, X. Venturing beyond Donor-Controlled Glycosylation: New Perspectives toward Anomeric Selectivity. *Acc. Chem. Res.* **2018**, *51* (3), 628–639.
- (5) Nigudkar, S. S.; Demchenko, A. V. Stereocontrolled 1,2-Cis Glycosylation as the Driving Force of Progress in Synthetic Carbohydrate Chemistry. *Chem. Sci.* **2015**, *6* (5), 2687–2704.
- (6) Demchenko, A. V. *Handbook of Chemical Glycosylation: Advances in Stereoselectivity and Therapeutic Relevance*; Wiley, 2008.
- (7) Bennett, C. S. Selective Glycosylations with Deoxy Sugars. In *Selective Glycosylations: Synthetic Methods and Catalysts*; Bennett, C. S., Ed.; Wiley-VCH Verlag GmbH & Co. KGaA, 2017; pp 277–295.
- (8) Bohé, L.; Crich, D. A Propos of Glycosyl Cations and the Mechanism of Chemical Glycosylation. *C. R. Chim.* **2011**, *14* (1), 3–16.
- (9) Crich, D. Mechanism of a Chemical Glycosylation Reaction. *Acc. Chem. Res.* **2010**, *43* (8), 1144–1153.

- (10) Adero, P. O.; Amarasekara, H.; Wen, P.; Bohé, L.; Crich, D. The Experimental Evidence in Support of Glycosylation Mechanisms at the  $S_N1-S_N2$  Interface. *Chem. Rev.* **2018**, *118* (17), 8242–8284.

- (11) van der Vorm, S.; Overkleeft, H. S.; van der Marel, G. A.; Codée, J. D. C. Stereoselectivity of Conformationally Restricted Glucosazide Donors. *J. Org. Chem.* **2017**, *82* (9), 4793–4811.

- (12) Frihed, T. G.; Bols, M.; Pedersen, C. M. Mechanisms of Glycosylation Reactions Studied by Low-Temperature Nuclear Magnetic Resonance. *Chem. Rev.* **2015**, *115* (11), 4963–5013.

- (13) Frihed, T. G.; Walvoort, M. T. C.; Codée, J. D. C.; van der Marel, G. A.; Bols, M.; Pedersen, C. M. Influence of O6 in Mannosylations Using Benzylidene Protected Donors: Stereoelectronic or Conformational Effects? *J. Org. Chem.* **2013**, *78* (6), 2191–2205.

- (14) Kaeothip, S.; Yasomane, J. P.; Demchenko, A. V. Glycosidation of Thioglycosides in the Presence of Bromine: Mechanism, Reactivity, and Stereoselectivity. *J. Org. Chem.* **2012**, *77* (1), 291–299.

- (15) Walvoort, M. T. C.; Lodder, G.; Mazurek, J.; Overkleeft, H. S.; Codée, J. D. C.; van der Marel, G. A. Equatorial Anomeric Triflates from Mannuronic Acid Esters. *J. Am. Chem. Soc.* **2009**, *131* (34), 12080–12081.

- (16) Liu, J.; Gin, D. Y. C2-Amidoglycosylation. Scope and Mechanism of Nitrogen Transfer. *J. Am. Chem. Soc.* **2002**, *124* (33), 9789–9797.

- (17) Garcia, B. A.; Gin, D. Y. Dehydrative Glycosylation with Activated Diphenyl Sulfonium Reagents. Scope, Mode of C(1)-Hemiacetal Activation, and Detection of Reactive Glycosyl Intermediates. *J. Am. Chem. Soc.* **2000**, *122* (18), 4269–4279.

- (18) Crich, D.; Sun, S. Are Glycosyl Triflates Intermediates in the Sulfoxide Glycosylation Method? A Chemical and  $^1\text{H}$ ,  $^{13}\text{C}$ , and  $^{19}\text{F}$  NMR Spectroscopic Investigation. *J. Am. Chem. Soc.* **1997**, *119* (46), 11217–11223.

- (19) van der Vorm, S.; Hansen, T.; Overkleeft, H. S.; van der Marel, G. A.; Codée, J. D. C. The Influence of Acceptor Nucleophilicity on the Glycosylation Reaction Mechanism. *Chem. Sci.* **2017**, *8* (3), 1867–1875.

- (20) Moumé-Pymbock, M.; Crich, D. Stereoselective C-Glycoside Formation with 2-O-Benzyl-4,6-O-Benzylidene Protected 3-Deoxy Gluco- and Mannopyranoside Donors: Comparison with O-Glycoside Formation. *J. Org. Chem.* **2012**, *77* (20), 8905–8912.

- (21) Codée, J. D. C.; Walvoort, M. T. C.; de Jong, A. R.; Lodder, G.; Overkleeft, H. S.; van der Marel, G. A. Mannuronic Acids: Reactivity and Selectivity. *J. Carbohydr. Chem.* **2011**, *30* (7–9), 438–457.

- (22) Beaver, M. G.; Woerpel, K. A. Erosion of Stereochemical Control with Increasing Nucleophilicity: O-Glycosylation at the Diffusion Limit. *J. Org. Chem.* **2010**, *75* (4), 1107–1118.

- (23) Walvoort, M. T. C.; Dinkelaar, J.; van den Bos, L. J.; Lodder, G.; Overkleeft, H. S.; Codée, J. D. C.; van der Marel, G. A. The Impact of Oxacarbenium Ion Conformers on the Stereochemical Outcome of Glycosylations. *Carbohydr. Res.* **2010**, *345* (10), 1252–1263.

- (24) Lucero, C. G.; Woerpel, K. A. Stereoselective C-Glycosylation Reactions of Pyranoses: The Conformational Preference and Reactions of the Mannosyl Cation. *J. Org. Chem.* **2006**, *71* (7), 2641–2647.

- (25) Crich, D.; Vinogradova, O. On the Influence of the C2–O2 and C3–O3 Bonds in 4,6-O-Benzylidene-Directed  $\beta$ -Mannopyranosylation and  $\alpha$ -Glucopyranosylation. *J. Org. Chem.* **2006**, *71* (22), 8473–8480.

- (26) Krumper, J. R.; Salamant, W. A.; Woerpel, K. A. Continuum of Mechanisms for Nucleophilic Substitutions of Cyclic Acetals. *Org. Lett.* **2008**, *10* (21), 4907–4910.

- (27) Zhu, X.; Kawatkar, S.; Rao, Y.; Boons, G. J. Practical Approach for the Stereoselective Introduction of  $\beta$ -Arabinofuranosides. *J. Am. Chem. Soc.* **2006**, *128* (36), 11948–11957.

- (28) Ishiwata, A.; Akao, H.; Ito, Y. Stereoselective Synthesis of a Fragment of Mycobacterial Arabinan. *Org. Lett.* **2006**, *8* (24), 5525–5528.

- (29) Nukada, T.; Bérces, A.; Wang, L.; Zgierski, M. Z.; Whitfield, D. M. The Two-Conformer Hypothesis: 2,3,4,6-Tetra-*O*-Methyl-Mannopyranosyl and -Glucopyranosyl Oxocarbenium Ions. *Carbohydr. Res.* **2005**, *340* (5), 841–852.
- (30) Larsen, C. H.; Ridgway, B. H.; Shaw, J. T.; Smith, D. M.; Woerpel, K. A. Stereoselective C-Glycosylation Reactions of Ribose Derivatives: Electronic Effects of Five-Membered Ring Oxocarbenium Ions. *J. Am. Chem. Soc.* **2005**, *127* (31), 10879–10884.
- (31) Ayala, L.; Lucero, C. G.; Romero, J. A. C.; Tabacco, S. A.; Woerpel, K. A. Stereochemistry of Nucleophilic Substitution Reactions Depending upon Substituent: Evidence for Electrostatic Stabilization of Pseudoaxial Conformers of Oxocarbenium Ions by Heteroatom Substituents. *J. Am. Chem. Soc.* **2003**, *125* (50), 15521–15528.
- (32) Romero, J. A. C.; Tabacco, S. A.; Woerpel, K. A. Stereochemical Reversal of Nucleophilic Substitution Reactions Depending upon Substituent: Reactions of Heteroatom-Substituted Six-Membered-Ring Oxocarbenium Ions through Pseudoaxial Conformers. *J. Am. Chem. Soc.* **2000**, *122* (1), 168–169.
- (33) Parent, J. F.; Deslongchamps, P. Bent Bonds ( $\tau$ ) and the Antiperiplanar Hypothesis, and the Reactivity at the Anomeric Center in Pyranosides. *Org. Biomol. Chem.* **2016**, *14* (47), 11183–11198.
- (34) Ardévol, A.; Rovira, C. The Molecular Mechanism of Enzymatic Glycosyl Transfer with Retention of Configuration: Evidence for a Short-Lived Oxocarbenium-Like Species. *Angew. Chem., Int. Ed.* **2011**, *50* (46), 10897–10901.
- (35) Iglesias-Fernández, J.; Hancock, S. M.; Lee, S. S.; Khan, M.; Kirkpatrick, J.; Oldham, N. J.; McAuley, K.; Fordham-Skelton, A.; Rovira, C.; Davis, B. G. A Front-Face “ $S_Ni$ ” Synthase Engineered from a Retaining “Double- $S_N2$ ” Hydrolase. *Nat. Chem. Biol.* **2017**, *13* (8), 874–881.
- (36) Beenakker, T. J. M.; Wander, D. P. A.; Offen, W. A.; Artola, M.; Raich, L.; Ferraz, M. J.; Li, K.-Y.; Houben, J. H. P. M.; van Rijssel, E. R.; Hansen, T.; et al. Carba-Cyclophellitols Are Neutral Retaining-Glucosidase Inhibitors. *J. Am. Chem. Soc.* **2017**, *139* (19), 6534–6537.
- (37) Martin, A.; Arda, A.; Désiré, J.; Martin-Mingot, A.; Probst, N.; Sinäy, P.; Jiménez-Barbero, J.; Thibaudeau, S.; Blériot, Y. Catching Elusive Glycosyl Cations in a Condensed Phase with HF/SbF<sub>5</sub> Superacid. *Nat. Chem.* **2016**, *8* (2), 186–191.
- (38) Elferink, H.; Severijnen, M. E.; Martens, J.; Mensink, R. A.; Berden, G.; Oomens, J.; Rutjes, F. P. J. T.; Rijs, A. M.; Boltje, T. J. Direct Experimental Characterization of Glycosyl Cations by Infrared Ion Spectroscopy. *J. Am. Chem. Soc.* **2018**, *140* (19), 6034–6038.
- (39) Mucha, E.; Marianski, M.; Xu, F. F.; Thomas, D. A.; Meijer, G.; von Helden, G.; Seeberger, P. H.; Pagel, K. Unravelling the Structure of Glycosyl Cations via Cold-Ion Infrared Spectroscopy. *Nat. Commun.* **2018**, *9* (1), 4174.
- (40) Novel corrections and functionals, including B3LYP-D3 and  $\omega$ B97XD, were also used and showed comparable results (see the SI for full details).
- (41) The effect of the solvent on the outcome of the addition reactions to the fuco- and rhamno-configured oxocarbenium ions **19** and **22**, respectively, has been investigated by performing the reactions in Et<sub>2</sub>O and MeCN. The outcome of these reactions was similar to the outcome of the reactions in DCM, with the 1,2-*cis*-addition products being formed as the sole anomer. These results are in line with the structures of the intermediate oxocarbenium ions, as revealed by the CEL maps of these ions in the respective solvents (see the SI for full details).
- (42) For ease of visualization, the Cremer–Pople globe is turned 180° with respect to its common representation, and both poles (the <sup>4</sup>C<sub>1</sub> and <sup>1</sup>C<sub>4</sub> structures) are omitted as these conformations are very high in energy.
- (43) Deslongchamps, P.; Dory, Y. L.; Li, S. 1994 R.U. Lemieux Award Lecture Hydrolysis of Acetals and Ketals. Position of Transition States along the Reaction Coordinates, and Stereoelectronic Effects. *Can. J. Chem.* **1994**, *72* (10), 2021–2027.
- (44) van Rijssel, E. R.; van Delft, P.; Lodder, G.; Overkleeft, H. S.; van der Marel, G. A.; Filippov, D. V.; Codée, J. D. C. Furanosyl Oxocarbenium Ion Stability and Stereoselectivity. *Angew. Chem., Int. Ed.* **2014**, *53* (39), 10381–10385.
- (45) van Rijssel, E. R.; van Delft, P.; van Marle, D. V.; Bijvoets, S. M.; Lodder, G.; Overkleeft, H. S.; van der Marel, G. A.; Filippov, D. V.; Codée, J. D. C. Stereoselectivity in the Lewis Acid Mediated Reduction of Ketofuranoses. *J. Org. Chem.* **2015**, *80* (9), 4553–4565.
- (46) Madern, J. M.; Hansen, T.; van Rijssel, E. R.; Kistemaker, H. A. V.; van der Vorm, S.; Overkleeft, H. S.; van der Marel, G. A.; Filippov, D. V.; Codée, J. D. C. Synthesis, Reactivity, and Stereoselectivity of 4-Thiofuranosides. *J. Org. Chem.* **2019**, *84* (3), 1218–1227.
- (47) Jensen, H. H.; Lyngbye, L.; Jensen, A.; Bols, M. Stereoelectronic Substituent Effects in Polyhydroxylated Piperidines and Hexahydropyridazines. *Chem. - Eur. J.* **2002**, *8* (5), 1218–1226.
- (48) Jensen, H. H.; Bols, M. Stereoelectronic Substituent Effects. *Acc. Chem. Res.* **2006**, *39* (4), 259–265.
- (49) Bucher, C.; Gilmour, R. Fluorine-Directed Glycosylation. *Angew. Chem., Int. Ed.* **2010**, *49* (46), 8724–8728.
- (50) Beaver, M. G.; Billings, S. B.; Woerpel, K. A. C-Glycosylation Reactions of Sulfur-Substituted Glycosyl Donors: Evidence against the Role of Neighboring-Group Participation. *J. Am. Chem. Soc.* **2008**, *130* (6), 2082–2086.
- (51) Codée, J. D. C.; Litjens, R. E. J. N.; den Heeten, R.; Overkleeft, H. S.; van Boom, J. H.; van der Marel, G. A. Ph<sub>2</sub>SO/Tf<sub>2</sub>O: A Powerful Promotor System in Chemoselective Glycosylations Using Thioglycosides. *Org. Lett.* **2003**, *5* (9), 1519–1522.
- (52) Addition reactions, in which L-fucose, L-rhamnose, and D-glucose *N*-phenyl trifluoroacetimidate donors were used in conjunction with a catalytic amount of TMSOTf (0.1 equiv.) and TES-D, proceeded with a similar stereochemical outcome (see the SI for full details).
- (53) Hagen, B.; Ali, S.; Overkleeft, H. S.; van der Marel, G. A.; Codée, J. D. C. Mapping the Reactivity and Selectivity of 2-Azidofucosyl Donors for the Assembly of *N*-Acetylglucosamine-Containing Bacterial Oligosaccharides. *J. Org. Chem.* **2017**, *82* (2), 848–868.
- (54) Guillemineau, M.; Auzanneau, F. I. Challenging Deprotection Steps During the Synthesis of Tetra- and Pentasaccharide Fragments of the Leallex Tumor-Associated Hexasaccharide Antigen. *J. Org. Chem.* **2012**, *77* (20), 8864–8878.
- (55) Mong, K. K. T.; Wong, C. H. Reactivity-Based One-Pot Synthesis of a Lewis Y Carbohydrate Hapten: A Colon–Rectal Cancer Antigen Determinant. *Angew. Chem.* **2002**, *114* (21), 4261–4264.
- (56) The experimental data of the model glycosylations of the monosubstituted pyranosyl donors were obtained from the work of Woerpel and co-workers (experimental conditions: allyltrimethylsilane (4.0 equiv), Lewis acid (BF<sub>3</sub>·OEt<sub>2</sub> or SnBr<sub>4</sub>; 1.0 equiv), pyranosyl-1-*O*-acetyl donor in DCM (0.15 M), –78 °C to room temperature.). The model glycosylations of the multisubstituted pyranosyl donors were done with preactivation conditions (experimental conditions: preactivation conditions; TES-D (2 equiv), Tf<sub>2</sub>O (1.3 equiv), Ph<sub>2</sub>SO (1.3 equiv), TTBP (2.5 equiv), pyranosyl-1-*S*-thiophenyl donors, DCM (0.05 M), –80 to –60 °C, 96 h.).
- (57) To keep the calculation time manageable, large protection groups (BnO–) were substituted with electronic comparable smaller groups (MeO–) (see the SI for full details).
- (58) Olah, G. A.; Parker, D. G.; Yoneda, N.; Pelizza, F. Oxyfunctionalization of Hydrocarbons. 1. Protolytic Cleavage-Rearrangement Reactions of Tertiary Alkyl Hydroperoxides with Magic Acid. *J. Am. Chem. Soc.* **1976**, *98* (8), 2245–2250.
- (59) van der Vorm, S.; van Hengst, J. M. A.; Bakker, M.; Overkleeft, H. S.; van der Marel, G. A.; Codée, J. D. C. Mapping the Relationship between Glycosyl Acceptor Reactivity and Glycosylation Stereoselectivity. *Angew. Chem., Int. Ed.* **2018**, *57* (27), 8240–8244.